INTERNATIONAL JOURNAL OF HYDROGEN ENERGY XXX (XXXX) XXX

ELSEVIER

Available online at www.sciencedirect.com

ScienceDirect

journal homepage: www.elsevier.com/locate/he

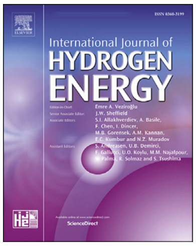

Theoretical understanding of stability of the oxygen electrode in a proton-conductor based solid oxide electrolysis cell

Yudong Wang*, Barbara Marchetti, Xiao-Dong Zhou**

Institute for Materials Research and Innovation, Department of Chemical Engineering, University of Louisiana at Lafayette, LA, 70504, USA

HIGHLIGHTS

- A proton-conductor based electrolysis cell significantly reduces μ_{O_2} and suppresses the delamination problem.
- The dependence of μ_{O_2} on the Faradaic efficiency is negligible with a typical proton-conducting electrolyte.
- Using high ionic conducting electrode and improving electrode kinetics further reduce μ_{O_2} and improve the electrode stability.

ARTICLE INFO

Article history:
Received 28 September 2022
Received in revised form
1 April 2023
Accepted 14 April 2023
Available online xxx

Keywords:
Proton conductor
Electrolyzer
Triple conducting electrode
Electrode stability
Oxygen chemical potential

ABSTRACT

The oxygen electrode in a proton-conductor based solid oxide cells is often a triple-conducting material that enables the transport and exchange of electrons (e^-), oxygen ions (O^{2-}), and protons (H^+), thus expanding active areas to enhance the oxygen electrode activity. In this work, a theoretical model was developed to understand stability of tri-conducting oxygen electrode by studying chemical potentials of neutral species (*i.e.*, μ_{O_2}, μ_{H_2}, and μ_{H_2O}) as functions of transport properties, operating parameters, and cell geometry. Our theoretical understanding shows that (1): In a conventional oxygen-ion based solid oxide cell, a high μ_{O_2} (thus high oxygen partial pressure) exists in the oxygen electrode during the electrolysis mode, which may lead to the formation of cracks at the electrode/electrolyte interface. While in a proton-conductor based solid oxide cell, the μ_{O_2} is reduced significantly, suppressing the crack formation, and resulting in improved performance stability (2). In a typical proton-conductor based solid oxide electrolyzer, the dependence of μ_{O_2} on the Faradaic efficiency is negligible. Hence, approaches to block the electronic current can improve the electrolysis efficiency while achieving stability (3). The difference of the μ_{O_2} (thus p_{O_2}) between the oxygen electrode and gas phase can be reduced by using higher ionic conducting components and improving electrode kinetics, which lead to further improvement of electrode stability.

---

* *Corresponding author.*
** *Corresponding author.*

E-mail addresses: Yudong.wang1@louisiana.edu (Y. Wang), zhou@louisiana.edu (X.-D. Zhou).

https://doi.org/10.1016/j.ijhydene.2023.04.148

Please cite this article as: Wang Y et al., Theoretical understanding of stability of the oxygen electrode in a proton-conductor based solid oxide electrolysis cell, International Journal of Hydrogen Energy, https://doi.org/10.1016/j.ijhydene.2023.04.148

List of symbols

$D_{O_2,k,eff}$	Effective Knudsen diffusion coefficient of oxygen ($m^2\ s^{-1}$)
$D_{O_2,H_2O,eff}$	Binary diffusion coefficient in the oxygen/steam mixture ($m^2\ s^{-1}$)
F	Faraday constant (96,485C mol^{-1})
ΔG_m^O	Molar Gibbs free energy change of O^{2-} oxidation (J mol^{-1})
ΔG_m^H	Molar Gibbs free energy change of H_2O oxidation (J mol^{-1})
i_0^H	Exchange current density from H_2O oxidation reaction. (A m^{-2})
i_{react}^H	Local current density generated from H_2O oxidation (A m^{-2})
i_0^O	Exchange current density from O^{2-} oxidation reaction. (A m^{-2})
i_{react}^O	Local current density generated O^{2-} oxidation (A m^{-2})
$I_{O^{2-}}$	Oxygen ionic current density (A m^{-2})
I_e	Electronic current density (A m^{-2})
I_{H^+}	Protonic current density (A m^{-2})
I_t	Total current density (A m^{-2})
l_{OE}	Oxygen electrode thickness (m)
M_{H_2O}	Molecular weight of water (kg mol^{-1})
M_{O_2}	Molecular weight of oxygen (kg mol^{-1})
N_{H_2O}	Steam molar flux (mol $m^{-2}\ s^{-1}$)
N_{O_2}	Oxygen molar flux (mol $m^{-2}\ s^{-1}$)
p_0	Pressure of atmosphere (Pa)
p_i	Partial pressure of species *i* (Pa)
R	Ideal gas constant (8.314 J $mol^{-1}\ K^{-1}$)
S^{OE}	The active area density in the oxygen electrode ($m^2\ m^{-3}$)
t_e	Electronic current fraction in the electrolyte
t_{H^+}	Protonic current fraction in the electrolyte
$t_{O^{2-}}$	Oxygen ion current fraction in the electrolyte
T	Absolute temperature (K)
x	Position away from the current collector (m)
y_{H_2O}	Steam molar fraction in the gas phase of the oxygen electrode
$y_{H_2O,0}$	Steam molar fraction in the inlet gas
y_{O_2}	Oxygen molar fraction in the gas phase of the oxygen electrode
$y_{O_2,0}$	Oxygen molar fraction in the inlet gas
α_a^O	Anodic charge transfer coefficient for O^{2-} oxidation
α_c^O	Cathodic charge transfer coefficient for O^{2-} oxidation
α_a^H	Anodic charge transfer coefficient for H_2O oxidation
α_c^H	Cathodic charge transfer coefficient for H_2O oxidation
ε	Porosity of the oxygen electrode
τ^{OE}	Tortuosity of the oxygen electrode
$\mu_{O_2}^g$	Chemical potential of oxygen in the gas phase (J mol^{-1})
$\mu_{O_2}^{OE}$	Chemical potential of oxygen in the oxygen electrode (J mol^{-1})
$\mu_{O_2}^0$	Chemical potential of oxygen under standard pressure (J mol^{-1})
μ_e	Chemical potential of electrons (J mol^{-1})
$\mu_{H_2}^{OE}$	Chemical potential of hydrogen in the oxygen electrode (J mol^{-1})
$\mu_{H_2}^0$	Chemical potential of hydrogen under standard pressure (J mol^{-1})
$\mu_{H_2O}^g$	Chemical potential of steam in the gas phase (J mol^{-1})
$\mu_{H_2O}^{OE}$	Chemical potential of steam in the oxygen electrode (J mol^{-1})
$\mu_{H_2O}^0$	Chemical potential of steam under standard pressure (J mol^{-1})
$\mu_{O_2}^{OE\vert El}$	Chemical potential of oxygen at the oxygen electrode/electrolyte interface (J mol^{-1})
$\tilde{\mu}_i$	Electrochemical potential of species *i* (J mol^{-1})
σ_i	The conductivity of species i in the oxygen electrode material (S m^{-1})
$\sigma_{e^-,eff}$	The effective electronic conductivity in the oxygen electrode (S m^{-1})
$\sigma_{H^+,eff}$	The effective protonic conductivity in the oxygen electrode (S m^{-1})
$\sigma_{O^{2-},eff}$	The effective oxygen ion conductivity in the oxygen electrode (S m^{-1})
Φ	Electrostatic potential (V)
φ	Electrical potential (V)
φ^{OE}	Electrical potential at the current collector, $x = 0$(V)

Introduction

While the share of renewable energy supply has gradually increased over the past few decades, novel energy storage technologies are needed for renewable energy to meet with the growing energy demand, due to the well-known intermittent nature of renewable energy sources. Reversible solid oxide cells (SOCs) are promising candidates for high-efficiency conversion of electricity to fuel, and *vice versa*, and could therefore aid to better utilize the intermittent surplus of energy provided by renewable sources. In this respect, hydrogen is a carbon-free energy carrier; this valuable chemical can be consumed as a fuel in the solid oxide fuel cell (SOFC) mode to produce electricity with net-zero carbon emissions [1]. Furthermore, the solid oxide electrolyzer cell (SOEC), *i.e.*, the reverse mode of the SOFC, can enable highly efficient electricity-to-hydrogen fuel conversion, thus effectively allowing to store renewable electricity. It is, therefore, that a sustainable SOEC for hydrogen production may well be the key to reversible energy storage.

SOECs are categorized into two primary types based on the major charge carriers in the electrolyte, *i.e.*, oxygen ion-conducting SOECs (*o*-SOECs) and proton-conducting SOECs (*p*-SOECs). The *o*-SOEC is a more mature technology cf. the *p*-SOECs, and generally requires to operate at relatively high

Please cite this article as: Wang Y et al., Theoretical understanding of stability of the oxygen electrode in a proton-conductor based solid oxide electrolysis cell, International Journal of Hydrogen Energy, https://doi.org/10.1016/j.ijhydene.2023.04.148

temperatures (750–900 °C) [2]. Although, high temperatures enable desired fast oxygen ion conduction, they may also lead to various issues within the SOEC, first and foremost, related to performance degradation [3]. On the other hand, the *p*-SOEC technology is leading the effort for hydrogen generation at intermediate temperatures (300 °C–700 °C), owing to the smaller ion size of proton cf. oxygen ion [4]. In such devices, steam is introduced and oxidized at the oxygen electrode, thus forming protons and oxygen [5]. Barium zirconates, barium cerates, or combined compositions are then employed as solid electrolytes in *p*-SOECs to conduct the so-generated protons to the fuel electrode, where hydrogen evolution occurs [4,6]. It is to be noted that, although termed proton conducting, these electrolytes may also conduct oxygen ion as well as promoting the formation of electronic defects (electron holes) [4,7]. In a typical *p*-SOECs, the hydrogen evolution reaction occurs at a Ni-containing fuel electrode, which is itself not exposed to steam in high concentration; the risk of Ni migration and agglomeration, which is often a drawback in *o*-SOFCs [8], is lower in *p*-SOECs.

The sluggish water oxidation kinetics and the durability issues of the oxygen electrode are the remaining obstacles for the large-scale deployment of *p*-SOECs [4,9,10]. Mixed-conducting oxygen electrodes offers significant concentrations of mobile protonic defects, oxygen vacancies and electron holes [11,12]. The mixed-conducting phase allows the water oxidation reaction to occur on the whole surface of the electrode, so that the reaction zone is extended and the overall reaction kinetics is faster [13–15]. Nernst–Planck formulation is widely used to study the defect transport across the p-SOC [16]. Considering mixed-conducting behavior of $La_{0.6}Sr_{0.4}Co_{0.2}Fe_{0.8}O_3$ in a p-SOC, the oxygen electrode still contributes the most to the voltage loss, as determined in recent simulations [17]. The protonic defects shows a peak concentration at the oxygen electrode/electrolyte interface based on the Nernst–Planck model of defect transport across the cell [18,19]. The change in chemical potential of electrically neutral species, which originates from the coupling among the transport of ionic and electronic defects, can induce degradation of oxygen electrode materials and electrode-electrolyte interfaces [20–23]. The stability of oxygen electrode is affected by both oxygen (p_{O_2}) and steam partial pressure (p_{H_2O}) [9]. High p_{O_2} values result in crack formation, which typically occurs in *o*-SOEC [24]. Some perovskite oxygen electrodes, for example $Ba_{0.6}Sr_{0.4}Co_{0.2}Fe_{0.8}O_3$, also tend to decompose or undergo microstructural changes under high steam atmosphere, which is often fed in the oxygen electrode of *p*-SOEC [4,10]. In this work, a model of the oxygen electrode is built, and, subsequently, the distributions of chemical potentials, p_{O_2} and p_{H_2O} are calculated. By investigating the relationship between chemical potential and the transport properties in the mix conducting electrode and electrolyte, the optimization of a stable oxygen electrode material is then illustrated.

Model development

To maximize the activity of a porous oxygen electrode, a triple conducting oxide is employed as the oxygen electrode material. As shown in Fig. 1, The electrode material can conduct oxygen ions, protons, and electrons [25–27]. Consequently, protons, oxygen ions and electrons (electron holes) can carry the electrical charges. The fluxes of these charge carriers are driven by the electrochemical potential gradients of protons ($\tilde{\mu}_{H^+}$), oxygen ions ($\tilde{\mu}_{O^{2-}}$), and electrons ($\tilde{\mu}_{e^-}$), respectively [22]. The $\tilde{\mu}_{e^-}$ is directly relared to the electrical potential (φ) that is a measurable variable (*i.e.*, a value that is read by a voltmeter):

$$\varphi = -\frac{\tilde{\mu}_{e^-}}{F} \tag{1}$$

The proton, oxygen ion and electron current densities (I_{H^+}, $I_{O^{2-}}$ and I_{e^-}) can be described as in Eqs. (2)–(4):

$$I_{H^+} = -\frac{\sigma_{H^+,eff}}{F}\frac{d\tilde{\mu}_{H^+}}{dx} \tag{2}$$

$$I_{O^{2-}} = \frac{\sigma_{O^{2-},eff}}{2F}\frac{d\tilde{\mu}_{O^{2-}}}{dx} \tag{3}$$

$$I_{e^-} = \frac{\sigma_{e^-,eff}}{F}\frac{d\tilde{\mu}_{e^-}}{dx} \tag{4}$$

where $\sigma_{H^+,eff}$, $\sigma_{O^{2-},eff}$, and $\sigma_{e^-,eff}$ are the effective protonic, oxygen ion and electronic conductivities at the oxygen electrode, F is the Faraday constant, and x is the position away from the

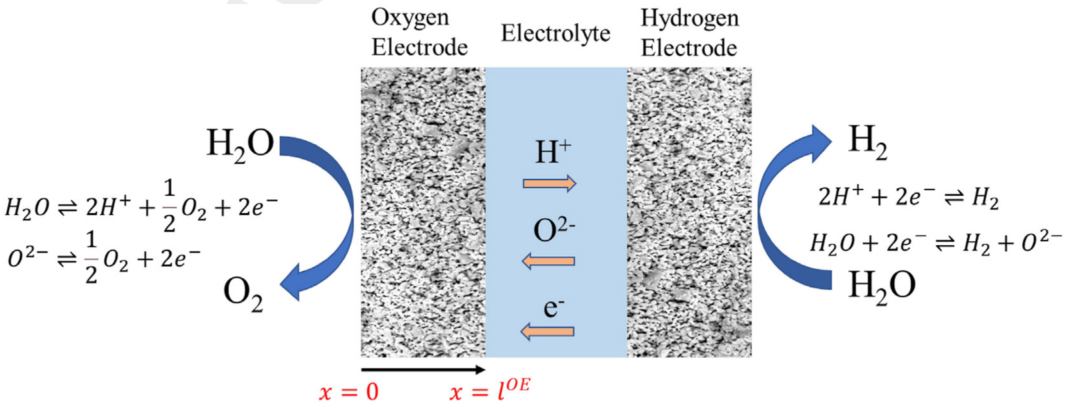

Fig. 1 – The schematics of a solid oxide electrolysis cell based on a mixed conducting electrolyte. The oxygen electrode is the focus of this study and is shown on the lefthand side, its thickness is l_{OE} (from $x = 0$ to $x = l_{OE}$).

Please cite this article as: Wang Y et al., Theoretical understanding of stability of the oxygen electrode in a proton-conductor based solid oxide electrolysis cell, International Journal of Hydrogen Energy, https://doi.org/10.1016/j.ijhydene.2023.04.148

current collector of the oxygen electrode. With Eq. (1), Eq. (4) can be rewritten as

$$I_{e^-} = -\sigma_{e^-,eff}\frac{d\varphi}{dx} \tag{5}$$

The electrochemical potential of a species i, $\tilde{\mu}_i$, is the sum of its chemical potential (μ_i) and the electro statistic potential (Φ), Eq. (6):

$$\tilde{\mu}_i = \mu_i + z_i F\Phi \tag{6}$$

$$\sigma_{i,eff} = \sigma_i\frac{1-\varepsilon}{\tau^{OE}} \tag{7}$$

where z_i is the number of charges carried by the species i, ε is the porosity of the oxygen electrode, and τ^{OE} is the tortuosity of the oxygen electrode.

In an SOEC, oxygen evolution reaction (OER) can occur at the surface of an oxygen electrode. OER may take place from the oxidation of oxygen ions (Eq. (8)) or water (Eq. (9)), with the acronym *OE* denoting the oxygen electrode:

$$O^{2-}(OE) \rightleftharpoons \frac{1}{2}O_2(g) + 2e^-(OE) \tag{8}$$

$$H_2O(g) \rightleftharpoons 2H^+(OE) + \frac{1}{2}O_2(g) + 2e^-(OE) \tag{9}$$

The driving force for the reaction shown in Eq. (8) is its molar Gibbs free energy change:

$$\Delta G_m^O = \frac{1}{2}\mu_{O_2}^g + 2\mu_{e^-} - \mu_{O^{2-}} \qquad [10]$$

Or

$$\Delta G_m^O = \frac{1}{2}\mu_{O_2}^g - 2F\varphi - \tilde{\mu}_{O^{2-}} \qquad [11]$$

In addition, oxygen can be formed inside the solid-state oxygen electrode.

$$O^{2-}(OE) \rightleftharpoons \frac{1}{2}O_2(OE) + 2e^-(OE) \qquad [12]$$

Considering reaction [12] under local equilibrium, at any given position in the oxygen electrode, the chemical potential of oxygen in the oxygen electrode gives

$$2\mu_{O^{2-}} = \mu_{O_2}^{OE} - 4\mu_{e^-} \qquad [13]$$

Rearranging Eq. [13]

$$\mu_{O_2}^{OE} = 2\tilde{\mu}_{O^{2-}} + 4F\varphi \qquad [14]$$

The molar Gibbs free energy change can be rewritten as,

$$\Delta G_m^O = \frac{1}{2}\left(\mu_{O_2}^g - \mu_{O_2}^{OE}\right) \qquad [15]$$

If $\mu_{O_2}^g < \mu_{O_2}^{OE}$, then $\Delta G_m^O < 0$, and primarily the OER occurs. On the contrary, for $\mu_{O_2}^g > \mu_{O_2}^{OE}$, it is derived that $\Delta G_m^O > 0$, that is, the reverse reaction, oxygen reduction reaction (ORR), occurs.

Similarly, the molar Gibbs free energy change reaction [9] can be written as:

$$\Delta G_m^H = \frac{1}{2}\mu_{O_2}^g + 2\mu_e + 2\mu_{H^+} - \mu_{H_2O}^g \qquad [16]$$

Or

$$\Delta G_m^H = \frac{1}{2}\mu_{O_2}^g - 2\varphi + 2\tilde{\mu}_{H^+} - \mu_{H_2O}^g \qquad [17]$$

Considering the reaction shown in Eq. (18) under equilibrium,

$$H_2(OE) \rightleftharpoons 2H^+(OE) + 2e^-(OE) \qquad [18]$$

The chemical potential of hydrogen in the oxygen electrode gives

$$\mu_{H_2}^{OE} = 2\mu_{H^+} - 2\mu_{e^-} \qquad [19]$$

Consider Eqs. (1) and (6), one can obtain:

$$\mu_{H_2}^{OE} = 2\tilde{\mu}_{H^+} - 2F\varphi \qquad [20]$$

Then, ΔG_m^H can be rewritten as in Eq. (21):

$$\Delta G_m^H = \frac{1}{2}\mu_{O_2}^g + \mu_{H_2}^{OE} - \mu_{H_2O}^g \qquad [21]$$

If $\mu_{O_2}^g > -2\mu_{H_2}^{OE} + 2\mu_{H_2O}^g$, then $\Delta G_m^H > 0$, and ORR occurs, while, if $\mu_{O_2}^g < -2\mu_{H_2}^{OE} + 2\mu_{H_2O}^g$, i.e., $\Delta G_m^H < 0$, then water oxidation reaction is favored. The chemical potentials of oxygen and steam in the gas phase of the porous oxygen electrode, *i.e.*, $\mu_{O_2}^g$ and $\mu_{H_2O}^g$, respectively, are functions of their respective concentrations (Eqs. (22) and (23)):

$$\mu_{O_2}^g = \mu_{O_2}^0 + RTln\left(y_{O_2}\right) \qquad [22]$$

$$\mu_{H_2O}^g = \mu_{H_2O}^0 + RTln\left(y_{H_2O}\right) \qquad [23]$$

Here, the gas phase is considered as an ideal gas mixture. The steam is carried by oxygen and fed to the oxygen electrode, then the sum of y_{O_2} and y_{H_2O} is unity by definition. The ORR or OER, which occur at the surface of the oxygen electrode, allow an exchange between ions and electrons:

$$\frac{dI_{O^{2-}}}{dx} = i_{react}^O \qquad [24]$$

$$\frac{dI_{H^+}}{dx} = i_{react}^H \qquad [25]$$

In Eq. (24) and (25), i_{react}^O and i_{react}^H are the current densities generated from reactions [8] and [9] in the region between x to x + dx, respectively. The Butler-Volmer-like equation is widely used to describe the electrode kinetics as functions of potentials:

$$i_{react}^O = i_0^O S^{OE}\left[\exp\left(-\frac{\alpha_a^O\Delta G_m^O}{RT}\right) - \exp\left(\frac{\alpha_c^O\Delta G_m^O}{RT}\right)\right] \qquad [26]$$

$$i_{react}^H = i_0^H S^{OE}\left[\exp\left(-\frac{\alpha_a^H\Delta G_m^H}{RT}\right) - \exp\left(\frac{\alpha_c^H\Delta G_m^H}{RT}\right)\right] \qquad [27]$$

Here, S^{OE} is the active area density in the oxygen electrode. Considering the conservation of charge, the electrical current in oxygen electrode is:

$$\frac{dI_{e^-}}{dx} = -\frac{dI_{H^+}}{dx} - \frac{dI_{O^{2-}}}{dx} = -i_{react}^O - i_{react}^H \qquad [28]$$

Besides, the oxygen flux, N_{O_2}, follows the dusty gas model [28]:

Please cite this article as: Wang Y et al., Theoretical understanding of stability of the oxygen electrode in a proton-conductor based solid oxide electrolysis cell, International Journal of Hydrogen Energy, https://doi.org/10.1016/j.ijhydene.2023.04.148

$$\frac{N_{O_2}}{D_{O_2,k,eff}}+\frac{\left(1-y_{O_2}\right)N_{O_2}-y_{O_2}N_{H_2O}}{D_{O_2,H_2O,eff}}=-\frac{p}{RT}\frac{dy_{O_2}}{dx} \qquad [29]$$

where $D_{O_2,k,eff}$ is the effective Knudsen diffusion coefficient of oxygen and N_{H_2O} denotes the steam flux. $D_{O_2,H_2O,eff}$ is the binary diffusion coefficient in the oxygen/steam mixture. From the Graham's Law, it follows that:

$$N_{O_2}\sqrt{M_{O_2}}+N_{H_2O}\sqrt{M_{H_2O}}=0 \qquad [30]$$

where M_{O_2} and M_{H_2O} represent the molecular weights of oxygen and water, respectively. Thus, it is derived that:

$$\frac{dy_{O_2}}{dx}=-\frac{RTN_{O_2}}{p_0}\left(\frac{1-\left(1-\sqrt{\frac{M_{O_2}}{M_{H_2O}}}\right)y_{O_2}}{D_{O_2,H_2O,eff}}+\frac{1}{D_{O_2,k,eff}}\right) \qquad [31]$$

From the balance of oxygen in the gas phase, the change in oxygen flux is equal to the oxygen that is generated or consumed in the oxygen electrode under steady state.

$$\frac{dN_{O_2}}{dx}=-\frac{i^O_{react}+i^H_{react}}{4F} \qquad [32]$$

From above analysis, Eqs. ((2)–(4), (24), (25), (28), (31), (32)) are the sets of 8 first order differential equations to be solved to obtain chemical potential distribution which requires 8 boundary conditions. We assume that the electrical current passing through the current collector is carried by electrons only, and then, we consider that, at the electrode/current collector interface ($x = 0$), the ionic currents should be 0.

$$I_{O^{2-}}=I_{H^+}=0\ (x=0) \qquad [33]$$

The gas is fed with The gas phase has the same composition within the electrolyte, then:

$$y_{O_2}=y_{O_2,0}(x=0) \qquad [34]$$

$$y_{H_2O}=y_{H_2O,0}=1-y_{O_2,0}(x=0) \qquad [35]$$

The electrical potential is defined as equal to 0 V at the current collector.

$$\varphi^{OE}=0(x=0) \qquad [36]$$

At the electrode/electrolyte interface ($x = l_{OE}$), the current densities should be continuous. The current densities carried by oxygen ions, protons and electrons should equal to the value in the electrolyte, which is a triple conducting oxide [29].

$$I_{O^{2-}}=I^{el}_{O^{2-}}=t_{O^{2-}}I^{el}_t(x=l_{OE}) \qquad [37]$$

$$I_{H^+}=I^{el}_{H^+}=t_{H^+}I^{el}_t(x=l_{OE}) \qquad [38]$$

$$I_{e^-}=I^{el}_{e^-}=t_{e^-}I^{el}_t\ (x=l_{OE}) \qquad [39]$$

Where $t_{O^{2-}}$, t_{H^+} and t_{e^-} are the fractions of oxygen-ion current, protonic current, and electronic current in the electrolyte, respectively. The electrolyte is dense and gas tight, so the oxygen flux is set as 0

$$N_{O_2}=0\ (x=l_{OE}) \qquad [40]$$

Table 1 – A list of variables and their magnitudes used in modeling the oxygen electrode of SOEC.

Parameters	Magnitudes
$D_{O_2,k,eff}$	1.442×10^{-6} [$m^2\ s^{-1}$]
$D_{O_2,H_2O,eff}$	1.674×10^{-7} [$m^2\ s^{-1}$]
i^H_0	0.5–100 [$A\ m^{-2}$]
i^O_0	0.5–100 [$A\ m^{-2}$]
I_t	0–20,000 [$A\ m^{-2}$]
l_{OE}	3×10^{-5} [m]
S^{OE}	4.5×10^6 [m^{-1}]
t_{e^-}	0.01–0.6
t_{H^+}	0.01–0.89
$t_{O^{2-}}$	0.01–0.89
T	873 [K]
$y_{H_2O,0}$	0.5
$y_{O_2,0}$	0.5
α^O_a	0.5
α^O_c	0.5
α^H_a	0.5
α^H_c	0.5
ε	0.4
τ^{OE}	4.5
σ_{H^+}	0.05–2 [$S\ m^{-1}$]
$\sigma_{O^{2-}}$	0.05–2 [$S\ m^{-1}$]

with the above boundary conditions (Eqs. (33) and (34) and (36)–(40)), the boundary value problem is solved with the bvp4c solver in Matlab. The magnitudes of parameters used in the model are listed in Table 1. Parameters, including total current density, protonic current percentage, Faradaic efficiency, ionic conductivities, and exchange current densities, are studied within the range provided in Table 1.

Result and discussion

Effect of total current density

By applying an anodic potential on the oxygen electrode, oxygen gas is generated from the electrode surface. Indeed, from our analysis on reactions shown in Eqs. (8) and (9), a higher oxygen chemical potential or a lower hydrogen chemical potential in the solid phase of the electrode (cf. the gas phase) allows oxygen formation. Fig. 2(a), (b) and (c) show the chemical potential of O_2, H_2, and H_2O in the solid phase for a *p*-SOEC ($t_{O^{2-}} = 0.05$, $t_{H^+} = 0.85$, and $t_{e^-} = 0.1$). The chemical potential of H_2O is defined by assuming an equilibrium between the oxygen ions and protons as the reaction in Eq. (41):

$$H_2O(OE)\rightleftharpoons 2H^+(OE)+O^{2-}(OE) \qquad [41]$$

The equilibrium gives rise to the following relation:

$$\mu^{OE}_{H_2O}=2\tilde{\mu}_{H^+}+\tilde{\mu}_{O^{2-}}=\mu^{OE}_{H_2}+\frac{1}{2}\mu^{OE}_{O_2} \qquad [42]$$

At equilibrium (a total current density of 0 A), $\mu^{OE}_{O_2}$, $\mu^{OE}_{H_2}$ and $\mu^{OE}_{H_2O}$ are uniform in the electrode, and equal to the respective chemical potentials in the gas phase. When the electrode is polarized, the chemical potential differences are created between the gas phase and solid phase, which result in an electrolysis current and oxygen generation. The electrode under a current range between 0–2 A/cm² is modeled to

Please cite this article as: Wang Y et al., Theoretical understanding of stability of the oxygen electrode in a proton-conductor based solid oxide electrolysis cell, International Journal of Hydrogen Energy, https://doi.org/10.1016/j.ijhydene.2023.04.148

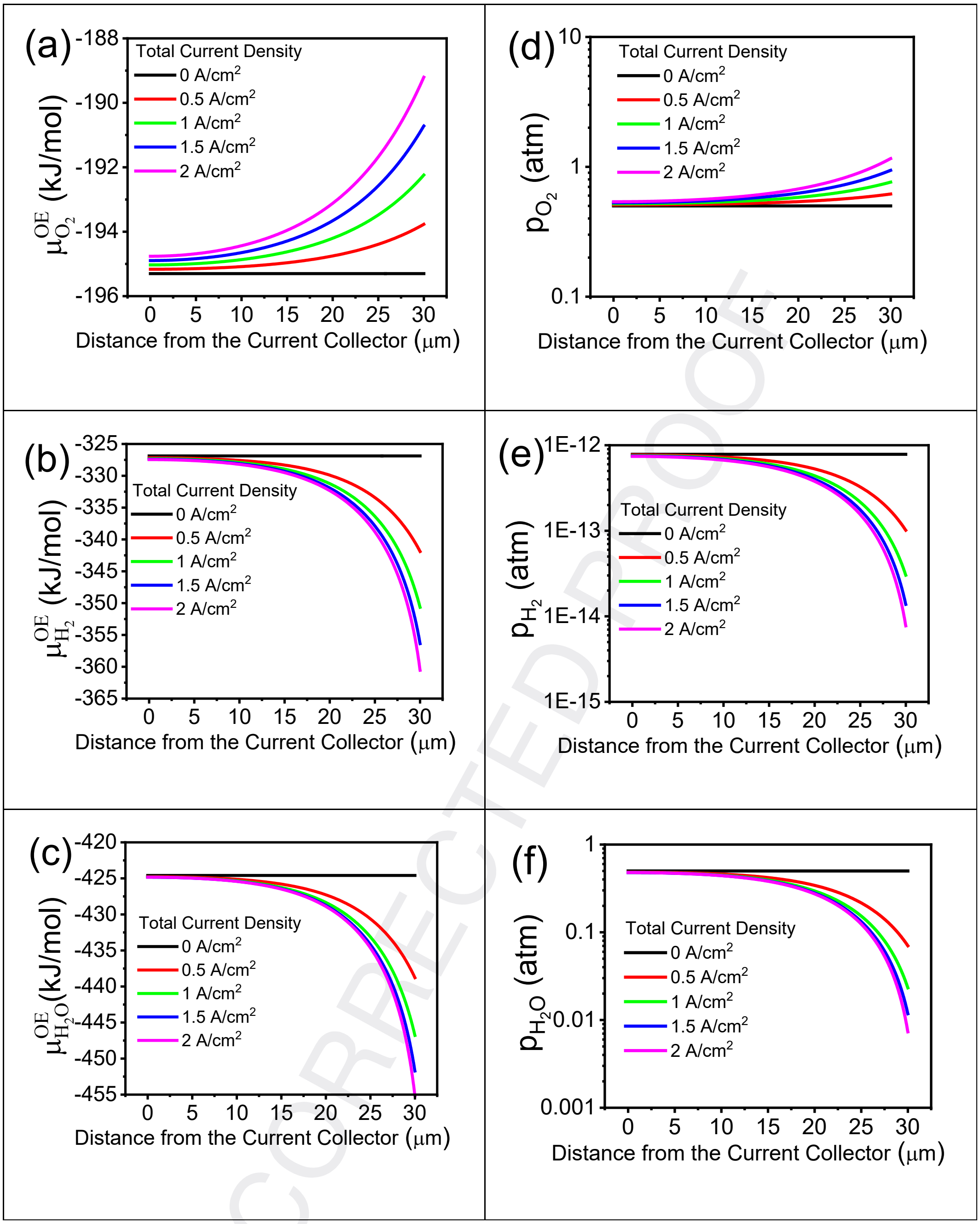

Fig. 2 – The chemical potentials of (a) oxygen, (b) hydrogen and (c) steam in the oxygen electrode as a function of distance from the current collector at different total current densities. The partial pressures of (d) oxygen, (e) hydrogen and (f) steam in the oxygen electrode as a function of distance from the current collector at different total current densities. ($t_{O^{2-}} = 0.05$, $t_{H^+} = 0.85$, and $t_{e^-} = 0.1$).

understand the impact of electrode polarization on the chemical potentials. A higher electron flux requires higher driving forces of the electrochemical reactions. Therefore, $\mu_{O_2}^{OE}$ increases, while $\mu_{H_2O}^{OE}$ and $\mu_{H_2}^{OE}$ decreases with an increasing electrolysis current [22]. In addition, the chemical potentials are not uniform along the thickness of the electrode. An active oxygen electrode usually has much higher electronic conductivity than the ion conductivity. The electrode reactions tend to occur at the interface between the electrode and electrolyte (i.e., at $x = l_{OE}$) to reduce the ion conduction pathway. The maximum $\mu_{O_2}^{OE}$ and minimum $\mu_{H_2O}^{OE}$ can be obtained at the OE/electrolyte interface. The change in chemical potential may shift the electrode material away from its stable region in the phase diagram, thus it may induce phase transition, decomposition or demixing [9]. In this context, the partial pressures of the species offer better interpretation and illustration of the chemical potentials. For a species i in an ideal gas mixture, its partial pressure (p_i) can be expressed in terms of its chemical potential (μ_i), as in Eq. (43):

Please cite this article as: Wang Y et al., Theoretical understanding of stability of the oxygen electrode in a proton-conductor based solid oxide electrolysis cell, International Journal of Hydrogen Energy, https://doi.org/10.1016/j.ijhydene.2023.04.148

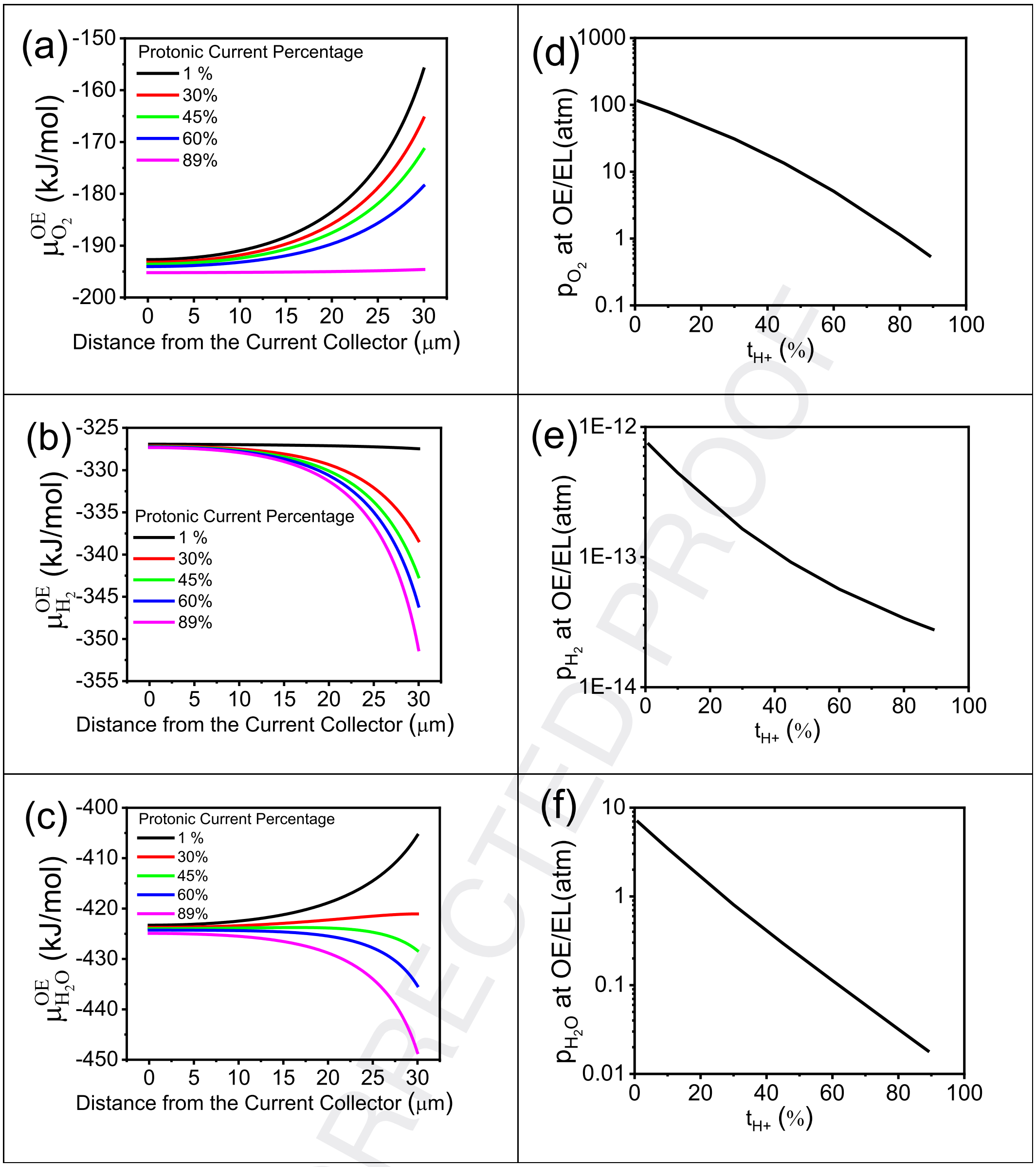

Fig. 3 – The chemical potentials of (a) oxygen, (b) hydrogen and (c) steam in the oxygen electrode with different protonic current densities. The partial pressures of (d) oxygen, (e) hydrogen and (f) steam at the OE and electrolyte interface as a function of the protonic current percentage in the electrolyte. ($I_t = 10,000\ A\ m^{-2}$, and $t_{e^-} = 0.1$).

$$p_i = p^0 \exp\left(\frac{\mu_i - \mu_i^0}{RT}\right) \qquad [43]$$

where p^0 is the reference pressure that is usually chosen as 1 atm, μ_i^0 is the chemical potential of species i at p^0 and temperature T. Hence, the p_{O_2}, p_{H_2}, and p_{H_2O} distributions along the thickness of the electrode can then be then plotted at various current densities as in Fig. 2(d)–(f). The oxygen partial pressure can reach a higher value than the gas phase at the OE/electrolyte interface (OE/EL), indicating that the interface is under highly oxidative conditions. The low electrolysis current density proves the stability of electrodes that are stable under steam-reach atmosphere [30,31]. On the other hand, the p_{H_2O} in the electrode reaches lower value near OE/EL, implying the stabilized region for the electrodes that is sensitive to high steam atmosphere.

Effect of protonic current percentage

In the previous analysis, the percentages of protonic current, oxygen ion current and electronic current are kept constant while only the total current is changed. However, the relative percentages of the partial current densities may vary depending on intrinsic properties of applied solid electrolyte, temperature, p_{O_2}, and p_{H_2O} [29,32,33]. For most proton conducting electrolyte, t_{H^+} increases with increasing and decreasing temperature and its value varies from 0 to 1. A very low t_{H^+} indicates that the electrolyte almost only conducts oxygen ion. Therefore, to investigate the behavior of the

Please cite this article as: Wang Y et al., Theoretical understanding of stability of the oxygen electrode in a proton-conductor based solid oxide electrolysis cell, International Journal of Hydrogen Energy, https://doi.org/10.1016/j.ijhydene.2023.04.148

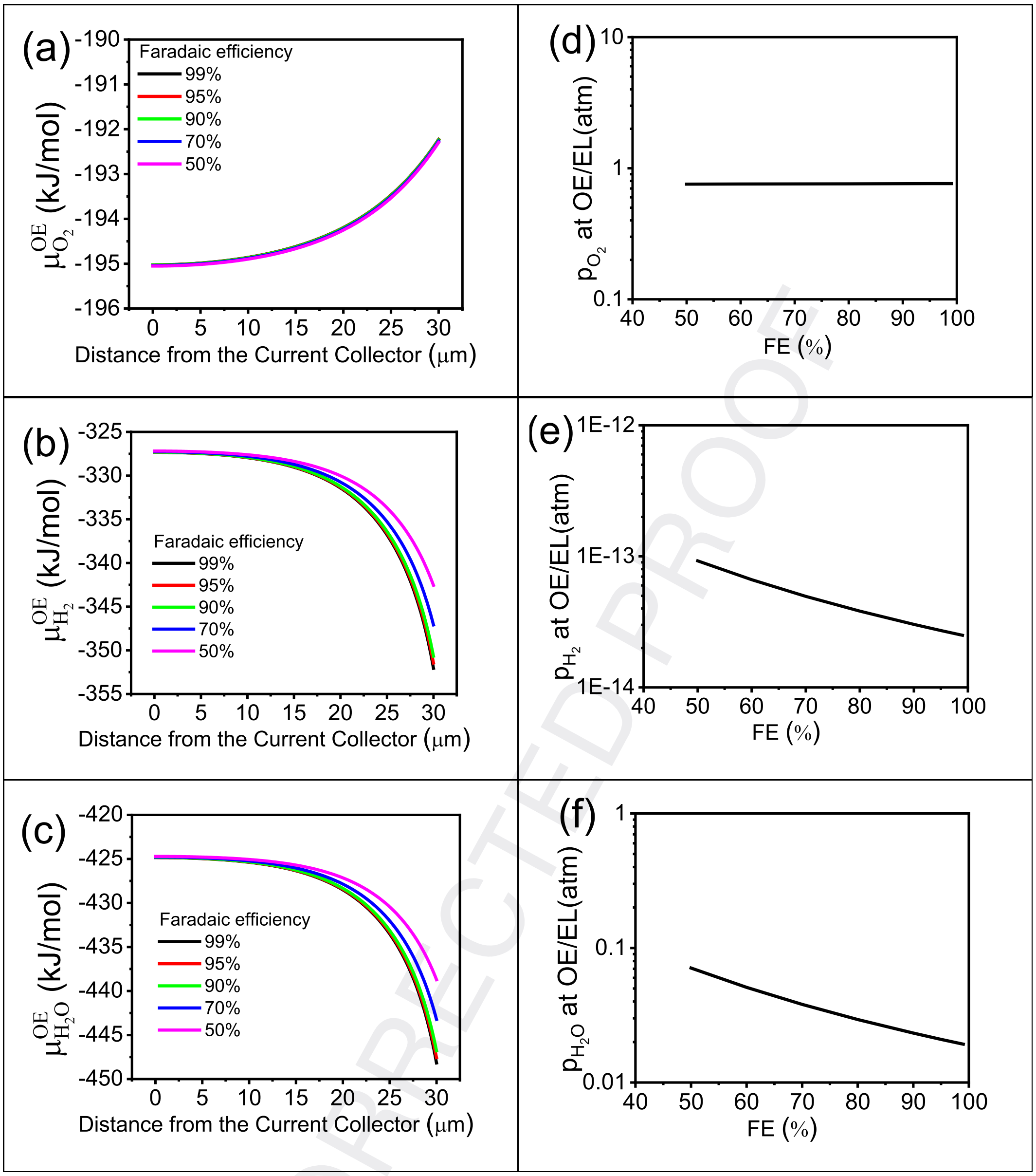

Fig. 4 – The chemical potentials of (a) oxygen, (b) hydrogen and (c) steam in the oxygen electrode with different Faradaic efficiencies. The partial pressures of (d) oxygen, (e) hydrogen and (f) steam at the OE and electrolyte interface as a function of the Faradaic efficiency for hydrogen production. ($I_t = 10,000\ A\ m^{-2}$, and $t_{O^{2-}} = 0.05$).

oxygen electrode when, for instance, the electrolyzer changes from *o*-SOEC to *p*-SOEC, total current can be kept constant. Furthermore, the percentage of electronic current is set at a fixed value of 10%, which is equivalent to a Faradaic efficiency of 90%. Fig. 3 (a) to (c) show the distribution of chemical potentials in the oxygen electrode with different protonic current ratios from the electrolyte. When the protonic current is low (1% of the total current density), the oxygen ion is the major carrier in the electrolyte and the electrolyzer behaves as a traditional *o*-SOEC. Under this case, reaction [8] is dominating, thus oxygen gas is mainly produced by the oxidation of oxygen ions, which results in a high internal oxygen partial pressure in the oxygen electrode, especially at OE/EL (Fig. 3(d)). This reason causes OE delamination in an *o*-SOEC, as in agreement with previous studies [20,23]. At the same time, in Fig. 3(b), it is shown that $\mu_{H_2}^{OE}$ stays almost constant in the electrode because only a negligeable fraction of protons is consumed and/or produced. Interestingly, $\mu_{H_2O}^{OE}$ also reaches high values at the OE/EL interface, owing to the equilibrium of reaction [41]. Concurrently, p_{H_2O} can be higher than the steam pressure in the gas phase. As the major carriers in the electrolyte transit from oxygen ions to protons, a lower $\mu_{O_2}^{OE}$ and a lower $\mu_{H_2}^{OE}$ are required. As Fig. 3 (d)–(f) shows, the partial pressure of oxygen, hydrogen and steam at OE/EL all decrease by 1–2 orders of magnitude with increasing t_{H^+}, in particular with p_{O_2} dropping from 114 atm to 0.5 atm with the increase of t_{H^+} from 1% to 89%. Therefore, allowing more protonic current across the cell helps reduce p_{O_2} and p_{H_2O} to suppress the degradation from the high pressures.

Effect of Faradaic efficiency

For *p*-SOEC, the electronic current leakage can be significant, which leads to a more serious concern especially at a high electrolysis current density. As a result, the Faradaic efficiency (FE) for hydrogen production may reach a relatively low value [34], while clearly higher FEs should always be pursued for high efficiency H_2-production. t_{e^-} in the electrolyte, which can vary from 0–1 under different conditions [29,32,33], determines FE values. Fig. 4 (a) to (c) illustrate the relation between the various chemical potential distributions and the cell FE with a constant $t_{O^{2-}} = 0.05$. With a constant oxygen-ion current, $\mu_{O_2}^{OE}$ is nearly independent on the FE, due largely to the very high σ_{e^-} and a very small φ drop. The $\mu_{O_2}^{OE}$ is determined by the electrochemical potential of oxygen ions ($\tilde{\mu}_{O^{2-}}$) and φ (Eq. (14)), which remains unvaried at different FEs. However, $\mu_{H_2}^{OE}$ and $\mu_{H_2O}^{OE}$ increase slightly for low FE because of the decrease in the protonic current in the electrolyte. While clearly p_{O_2} remains constant, the increase in $\mu_{H_2}^{OE}$ and $\mu_{H_2O}^{OE}$ results in an increase of p_{H_2} and p_{H_2O} of about one order of magnitude (Fig. 4d–f).

Ionic conductivities

The mix conducting behavior is the key to improve the electrochemical activity of the electrode. Fig. 5 (a) to (c) show how the proton conductivity affects the chemical potential distributions, while the effects of oxygen ion conductivity are illustrated in Fig. 5 (d)–(f). As shown in Fig. 5(a), the $\mu_{O_2}^{OE}$ is not

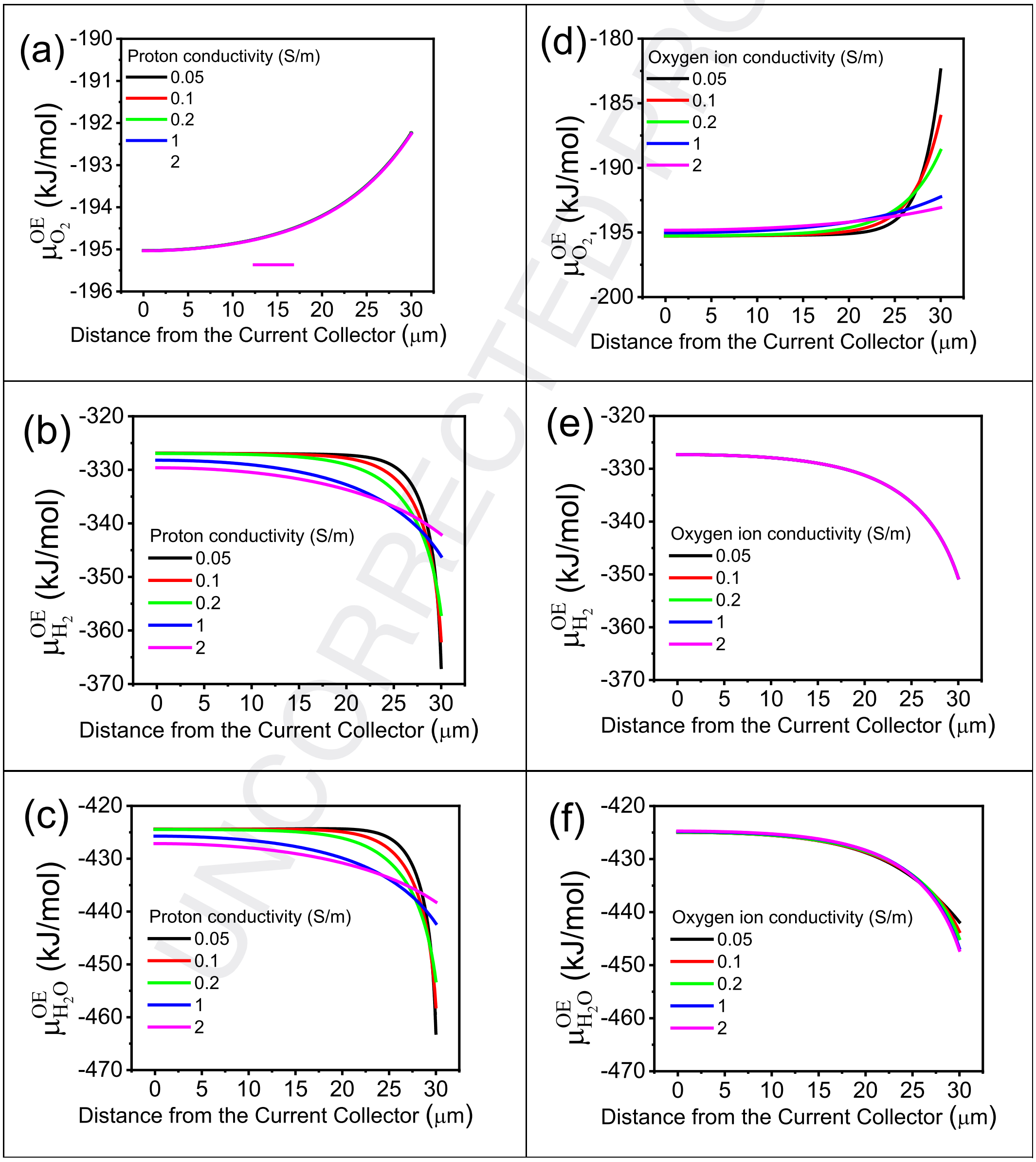

Fig. 5 – The chemical potentials of (a) oxygen, (b) hydrogen and (c) steam in the oxygen electrode as a function of the distance from the current collector with different protonic conductivities. The chemical potentials of (d) oxygen, (e) hydrogen and (f) steam in the oxygen electrode as a function of the distance from the current collector with different oxygen ion conductivities. ($I_t = 10,000\ A\ m^{-2}$, $t_{H^+} = 0.85$, $t_{O^{2-}} = 0.05$ and $t_{e^-} = 0.1$).

Please cite this article as: Wang Y et al., Theoretical understanding of stability of the oxygen electrode in a proton-conductor based solid oxide electrolysis cell, International Journal of Hydrogen Energy, https://doi.org/10.1016/j.ijhydene.2023.04.148

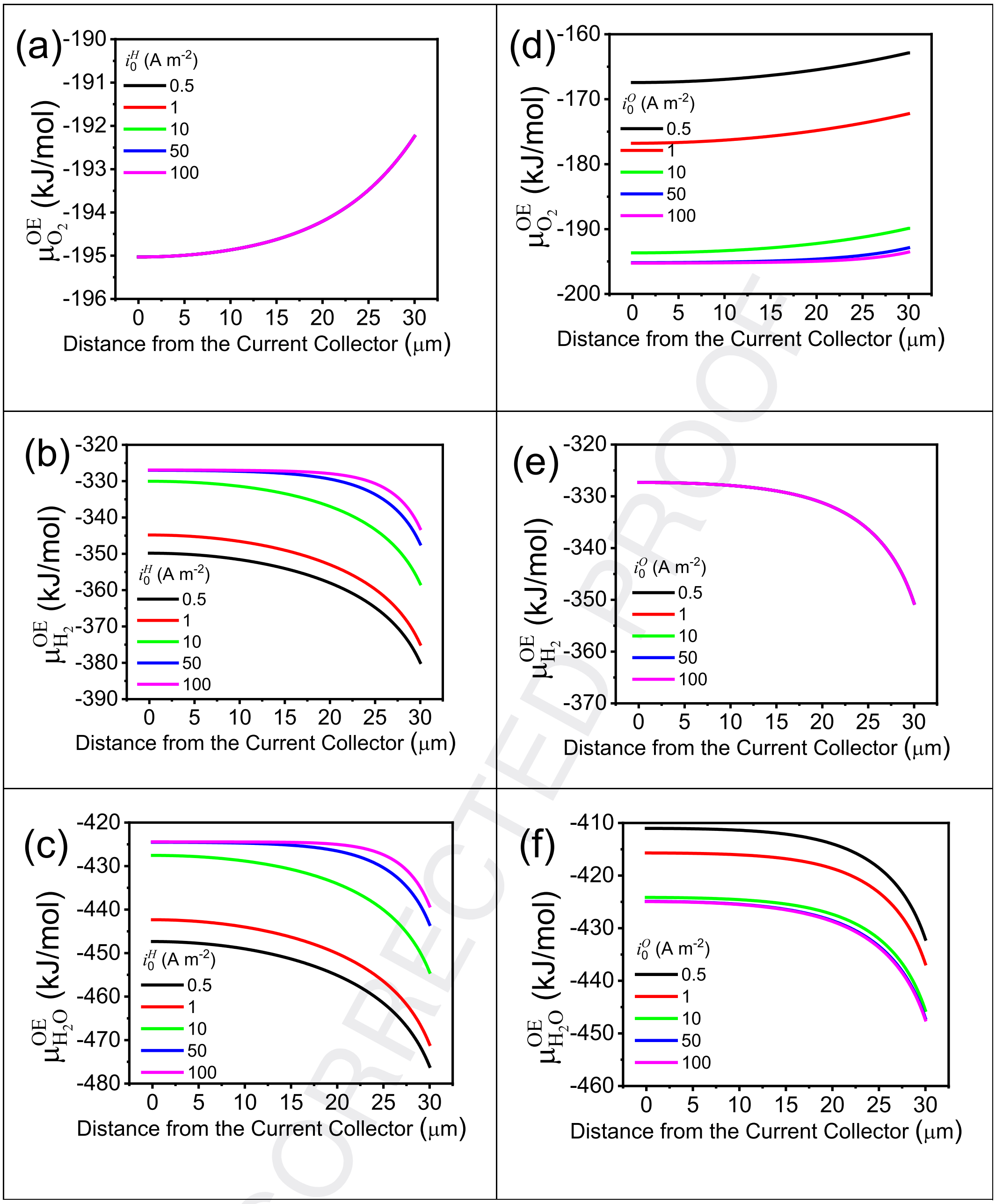

Fig. 6 – The chemical potentials of (a) oxygen, (b) hydrogen and (c) steam in the oxygen electrode as a function of the distance from the current collector with different exchange current densities for H_2O oxidation (i_0^H). The chemical potentials of (d) oxygen, (e) hydrogen and (f) steam in the oxygen electrode a function of the distance from the current collector with different exchange current densities for O^{2-} oxidation (i_0^O). ($I_t = 10,000\ A\ m^{-2}$, $t_{H^+} = 0.85$, $t_{O^{2-}} = 0.05$ and $t_{e^-} = 0.1$).

affected by σ_{H^+} as the O^{2-} current in the electrolyte is set to be constant. Analogously, $\mu^{OE}_{H_2}$ does not depend on $\sigma_{O^{2-}}$ as shown in Fig. 5 (e). The oxygen evolution reaction involves the transport of three different species, including gas, ions, and electrons. Therefore, the reaction likely occurs at the tiple-phase boundary, where the electrolyte, the oxygen electrode and gas phase meet. The mix conducting oxygen electrode allows the expansion of reaction zone from OE/EL to all the active surface of an oxygen electrode. The reaction zone reaches the current collector/oxygen electrode interface with high σ_{H^+} (>1 S/m). By increasing the protonic conductivity, the electrochemical driving force, ΔG^H_m, decreases near the OE/EL interface while it increases in the bulk phase due to the extended reaction zone. Therefore, $\mu^{OE}_{H_2}$ and $\mu^{OE}_{H_2O}$ increase near OE/EL while decreases in the bulk phase according to Eqs. (21) and (42). When a material with a higher $\sigma_{O^{2-}}$ is applied, $\mu^{OE}_{O_2}$ and $\mu^{OE}_{H_2O}$ near OE/EL are reduced, so as the p_{O_2} and p_{H_2O}. Hence, high ionic conductivities offer a high efficiency and the improved stability of the oxygen electrode. The triple-conducting oxygen electrode is mostly reported with extend durability [26,35,36].

Please cite this article as: Wang Y et al., Theoretical understanding of stability of the oxygen electrode in a proton-conductor based solid oxide electrolysis cell, International Journal of Hydrogen Energy, https://doi.org/10.1016/j.ijhydene.2023.04.148

Electrochemical kinetics

In this model, the Butler-Volmer equations are applied to describe the two electrochemical reactions occurring at the oxygen electrode. Important parameters to characterize the electrode kinetics are the exchange current densities, which are inversely proportional to the electrode polarization resistance. The corresponding results of our analysis are illustrated in Fig. 6(a)–(f). By increasing i_0^H from 0.5 to 100 A m^{-2}, $\mu_{H_2}^{OE}$ increases substantially at all points in the oxygen electrode while p_{H_2} increases from 5.38×10^{-16} to 2.5×10^{-13} atm, owing to the lower overpotential needed to generate the equivalent current density. Again, $\mu_{O_2}^{OE}$ remains constant resulting in enhanced activity towards steam oxidation, while $\mu_{H_2O}^{OE}$ increases by considering the contribution of $\mu_{O_2}^{OE}$ and $\mu_{H_2}^{OE}$, which is not favored for unstable oxygen electrode under high steam concentration. On the other hand, increasing i_0^O from 0.5 to 100 A m^{-2} results in higher $\mu_{O_2}^{OE}$, higher $\mu_{H_2O}^{OE}$ and constant $\mu_{H_2}^{OE}$, with p_{O_2} decreasing from 43.6 atm to 0.563 atm. Though oxygen ion only carries 5% charges, improving oxygen ion oxidation remains an important approach to reduce p_{O_2} value near the electrolyte, in order decreasing stress in proximity of the OE/electrolyte interface. Zhou et al. reported that the exsolved BaCoO3 nanoparticles improve the OER activity on the electrode surface and enhance i_0^O and i_0^H. The stability of the PBCC oxygen electrode benefits from the improved activity of the electrode surface [27].

Conclusion

In this work, a model was developed, aiming at the theoretical understanding of the interfacial stability between the oxygen electrode and electrolyte in a proton-conductor based solid oxide electrolysis cell. In the model here presented, the chemical potentials and partial pressures of oxygen, hydrogen, and steam are calculated by considering the transport of oxygen ion, proton and electrons in the oxygen electrode. The transition from oxygen ion-conducting to proton-conducting SOEC (*o*-SOEC and *p*-SOEC respectively) reduces the local partial pressure of O_2 in proximity of the electrolyte/electrode interface and reduces the stress along the boundary. In addition, higher ion conductivities and improved electrode kinetics reduce the overpotential in *p*-SOEC electrode and suppress the difference between chemical potentials in the oxygen electrode and in the electrolyte, which maintains the oxygen electrode material under the stable region and avoids high mechanical stress, thus to improving the durability of SOECs.

Declaration of competing interest

The authors declare that they have no known competing financial interests or personal relationships that could have appeared to influence the work reported in this paper.

Acknowledgement

We would like to thank the U.S. Department of Energy for the support of this work by the Office of Fossil Energy and Carbon Management under DE-FE0032110. Part of this work is supported by the Advanced Manufacturing Office of the Office of Energy Efficiency and Renewable Energy of the U.S. Department of Energy under DE-EE0009421 and National Science Foundation under NSF-2119688.

REFERENCES

[1] Hauch A, Küngas R, Blennow P, Hansen AB, Hansen JB, Mathiesen BV, Mogensen MB. Science 2020;370:eaba6118.
[2] Nechache A, Hody S. Renew Sustain Energy Rev 2021;149:111322.
[3] Wang Y, Li W, Ma L, Li W, Liu X. J Mater Sci Technol 2020;55:35.
[4] Duan C, Huang J, Sullivan N, O'Hayre R. Appl Phys Rev 2020;7:011314.
[5] Medvedev D. Int J Hydrogen Energy 2019;44:26711.
[6] Bi L, Boulfrad S, Traversa E. Chem Soc Rev 2014;43:8255.
[7] Yang L, Wang S, Blinn K, Liu M, Liu Z, Cheng Z, Liu M. Science 2009;326:126.
[8] Hjalmarsson P, Sun X, Liu Y-L, Chen M. J Power Sources 2014;262:316.
[9] Tarutin AP, Lyagaeva JG, Medvedev DA, Bi L, Yaremchenko AA. J Mater Chem 2021;9:154.
[10] Wang W, Medvedev D, Shao Z. Adv Funct Mater 2018;28:1802592.
[11] Zhou Y, Liu E, Chen Y, Liu Y, Zhang L, Zhang W, Luo Z, Kane N, Zhao B, Soule L, Niu Y, Ding Y, Ding H, Ding D, Liu M. ACS Energy Lett 2021;6:1511.
[12] Xu X, Pan Y, Zhong Y, Ran R, Shao Z. Mater Horiz 2020;7:2519.
[13] Tao Z, Fu M, Liu Y, Gao Y, Tong H, Hu W, Lei L, Bi L. Int J Hydrogen Energy 2022;47:1947.
[14] Zhou C, Sunarso J, Song Y, Dai J, Zhang J, Gu B, Zhou W, Shao Z. J Mater Chem 2019;7:13265.
[15] Song Y, Chen Y, Wang W, Zhou C, Zhong Y, Yang G, Zhou W, Liu M, Shao Z. Joule 2019;3:2842.
[16] Zhu H, Kee RJ. Int J Hydrogen Energy 2016;41:2931.
[17] Yan D, Wang W, Li R, Jiang S, Lu L, Levtsev A, Chen D. Appl Sci 2022;12:3889.
[18] Zhu H, Kee RJ. J Electrochem Soc 2017;164:F1400.
[19] Wrubel JA, Gifford J, Ma Z, Ding H, Ding D, Zhu T. Int J Hydrogen Energy 2021;46:11511.
[20] Virkar AV. Int J Hydrogen Energy 2010;35:9527.
[21] Virkar AV. J Power Sources 2009;194:753.
[22] Virkar AV. Int J Hydrogen Energy 2012;37:12609.
[23] Wang Y, Virkar AV, Khonsari MM, Zhou X-D. J Electrochem Soc 2022;169:044529.
[24] Mawdsley JR, David Carter J, Jeremy Kropf A, Yildiz B, Maroni VA. Int J Hydrogen Energy 2009;34:4198.
[25] Tian H, Li W, Ma L, Yang T, Guan B, Shi W, Kalapos TL, Liu X. ACS Appl Mater Interfaces 2020;12:49574.
[26] Ding H, Wu W, Jiang C, Ding Y, Bian W, Hu B, Singh P, Orme CJ, Wang L, Zhang Y. Nat Commun 2020;11:1.
[27] Zhou Y, Liu E, Chen Y, Liu Y, Zhang L, Zhang W, Luo Z, Kane N, Zhao B, Soule L. ACS Energy Lett 2021;6:1511.
[28] Matsuzaki K, Shikazono N, Kasagi N. J Power Sources 2011;196:3073.

Please cite this article as: Wang Y et al., Theoretical understanding of stability of the oxygen electrode in a proton-conductor based solid oxide electrolysis cell, International Journal of Hydrogen Energy, https://doi.org/10.1016/j.ijhydene.2023.04.148

[29] Zhu H, Ricote S, Duan C, O'Hayre RP, Kee RJ. J Electrochem Soc 2018;165:F845.

[30] Bausá N, Solís C, Strandbakke R, Serra JM. Solid State Ionics 2017;306:62.

[31] Li W, Guan B, Ma L, Hu S, Zhang N, Liu X. J Mater Chem 2018;6:18057.

[32] Heras-Juaristi G, Pérez-Coll D, Mather GC. J Power Sources 2017;364:52.

[33] Zhu H, Ricote S, Duan C, O'Hayre RP, Tsvetkov DS, Kee RJ. J Electrochem Soc 2018;165:F581.

[34] Zhu H, Ricote S, Kee RJ. J Phys: Energy 2022;4:014002.

[35] Jing J, Lei Z, Zheng Z, Wang H, Zhang P, Wang Z, Xu H, Yang Z. Int J Hydrogen Energy 2022. Q5

[36] Duan C, Kee R, Zhu H, Sullivan N, Zhu L, Bian L, Jennings D, O'Hayre R. Nat Energy 2019;4:230.

Please cite this article as: Wang Y et al., Theoretical understanding of stability of the oxygen electrode in a proton-conductor based solid oxide electrolysis cell, International Journal of Hydrogen Energy, https://doi.org/10.1016/j.ijhydene.2023.04.148